A New Design Approach for a Hybrid Monopole to Achieve Increased Ultrawide Bandwidth

Debatosh Guha, Debarati Ganguly, Sumesh George, Chandrakanta Kumar, Mailadil T. Sebastian, and Yahia M. M. Antar

A design approach has been explored and successfully demonstrated to achieve an improved gain of a hybrid monopole maintaining its optimum achievable bandwidth. This challenge has been resolved based on the knowledge acquired in earlier investigations. A three-segment composite dielectric ring resonator (DRR) has been designed and fabricated. This, along with a vertical monopole, promises about 137% (5.4:1) matching bandwidth with consistent monopole-like radiation and 6–10-dBi gain over the entire band. Two sets of customized prototypes have been realized and experimentally validated to furnish the predicted characteristics in transmit and receive modes, both in frequency and time domain.

DRR DEVELOPMENT: A CHRONOLOGY

The hybrid configuration of an electric monopole and a DRR has been known as an ultrawideband (UWB) monopole-antenna since [1] and [2]. This simple design approach of achieving monopole-type radiation over ultrawide bandwidth attracted many research groups who subsequently developed several variants over a period of time [3]–[9]. The chronology has been furnished in Table 1, which clearly indicates a trend in the increase of the operating bandwidth; the maxi- mum reported value being 138–140% [8], [9]. But it is interesting to note that their gain values are confined with- in 4–5 dBi, except in one case [6] in which it reaches up to 6 dBi. Earlier designs exploited strategic shaping of a DRR or monopole to allow closely spaced multiple resonances resulting in UWB operation.

This composite design approach explores an improvement in gain without any compromise in the maxi- mum achievable bandwidth and also demonstrates time-domain responses for this class of UWB antennas for the first time. A design clue has been extracted from the earlier studies and thoroughly discussed. This has resulted in a three-element composite DRR that has been critically designed, fabricated in our material laboratory, and experimentally studied. It prom- ises 6–10-dBi gain over 137% match- ing bandwidth. The physical insight into the accommodating higher reso- nant modes has also been discussed to facilitate further developments, especially for realizing a compact UWB sensor for electromagnetic interfer- ence and defense applications.

PROPOSED DESIGN AND CONFIGURATION

The clue to enhancing the gain is evident in Table 1:

1) The two-element DRR [6] offers maximum gain.

2) The dielectric body in [6] covers almost the entire height of the monopole and causes a much larger radiating sur- face compared to other designs.

3) The configuration [6] allows as many as four closely spaced resonances.

We have been guided by this set of observations and have intuitively con- ceived a three-element composite design of a DRR that owes its evolution to three of its predecessors: [1], [6], and [8]. The idea is depicted in Figure 1, and the structure details are provided in Figure 2. The pawn-shaped DRR [Figure 1(a)] with a high gain [6] was improvised in [8] [Figure 1(b)], promising a larger matching bandwidth. We, therefore, have developed it further by introducing an annular ring [Fig- ure 1(c)] [1]. The ring is sandwiched between two cones and looks like a mushroom [Figure 1(d)].

The proper combination of ε_{r1}, ε_{r2}, ε_{r3} of the mushroom-shaped DRR introduces six monopole-like resonances, two additional resonances over and above those provided by earlier configurations [6], [8]. We have followed [6] in selecting the lower cutoff frequency, which is determined by the first resonance f_1 of the standalone monopole with length $l = \lambda/4 = c/4f_1$ = 11 mm, c being the velocity of light in free space. The radius of the bare monopole chosen as r = 0.65 mm complies with the commercially available standard radius of a subminiature version A probe pin [6]. The height of each DRR segment was initially considered as 4 mm to cover l (= 11 mm).

The DRR permittivity has been deliberately reduced by about 25%, i.e., ε_{r1}, ε_{r2}, $\varepsilon_{r3} \leq 7.5$, to achieve a higher gain. As examined in [6], the electro- magnetic coupling between the monopole and the DRR is controlled by either s or b (= r +s), and, therefore, the optimum choice of b =1.5 mm [6] has been followed. The DRR dimensions have been initially chosen as $L_{DR2} \approx 8$ mm as in [8], $L_{DR1} \approx 2L_{DR2}$, and $L_{DR3} \approx 3L_{DR2}$. The permittivity values vary over 3–7 to examine their composite effect on matching bandwidth, and the ultimate choices are ε_{r1} =7, ε_{r2} =5, and ε_{r3} =4. This multisegment composite structure has been thoroughly investigated through a series of systematic studies to achieve the best possible design parameters.

DESIGN INSIGHT

The multiple resonances marked as f_1 -f_6 in Figure 3 have been identified. First, two resonances due to the standalone monopole closely correlate f_1 and f_5. The value of f_4 (12.5 GHz) exactly coincides with the DRR-alone, whereas its first higher mode (near 20 GHz) indicates its closeness to f_6.

Figure 4 searches for f_2 and f_3. The change in S_{11} due to sequential loading by DR1–DR3 indicates that the resonance near f_2 (7.3 GHz) is actually a contribution of DR1, which becomes prominent with DR1 + DR2. Until now, no trace of f_3 is revealed. After adding DR3, the resonance at f_3 becomes prominent, and f_2 appears to be consistent at the same frequency. Each represents an equivalent l/4 monopole with a reduced electrical length $l_{eq} < l$. This is caused by the presence of the DRR surrounding the monopole l. The same has been visually demonstrated in Figure 5. The stronger effect of dielectric loading is apparent at f_3 [Figure 5(b)] compared to that in f_2 [Figure 5(a)]. The calculated $l_{eq\,(f_3)} = c/4\,f_3 = 0.67l$, which exactly corroborates the result in [2] showing l_{eq} [2] =0.66l. This is the first time that someone has obtained an additional resonance by an additional reduced height monopole with $l_{eq(f_2)} = 0.934l$. We, therefore, can claim this as an important feature of the present design, causing wide impedance matching.

To ensure that all the resonances bear monopole-like fields, we have examined their individual E-plane (i.e., their vertical plane) radiations as shown in Figure 6. Here, the monopole-like pattern is evident, although the peak gain of the resonances varies in magnitude as well as angle of occurrence. The figure shows that at 23.6 GHz, the gain has increased up to 10 dBi higher. Wide frequency range antennas often have varying radiation patterns. However, the proposed antenna seems to maintain a good monopole- type radiation over the entire operating frequency range. The higher order mode in the DRR causes the gain to increase

by as much as 10 dBi, which in turn confirms our above identifications. Although a 10-dBi gain is achieved at the highest resonance, the average gain appearing around 60° (the angle of practical use) is in the range of 3–6 dBi, which is acceptable.

PROTOTYPES AND EXPERIMENTAL VERIFICATION

Two sets of prototypes bearing identical dimensions and other parameters were realized for experimental studies. We prepared customized dyes for the respective DRR units, and the materials with specified values were processed in our material science lab- oratory. A polymer ceramic composite was used. Strontium titanate ($SrTiO_3$), which has high permittivity, has been used as the filler, and polyethylene has been used as the polymer base for its low melting point of 160 °C [10].

An $SrTiO_3$ ceramic is prepared by a solid state ceramic route, and the polymer ceramic composite is pre- pared by melt-mixing using a kneading machine. The resultant composite is hot pressed to form a thin sheet. Its properties are measured using split- post dielectric resonator techniques. The desired permittivity values are achieved by varying the volume fraction of the filler loading.

The experimental results have been obtained using Agilent's Network Analyzer E8363B and an automated anechoic chamber. Figure 7 shows the measurement set up, while Figure 8 shows both the simulated and measured S_{11} values of both prototype A and B. The excellent mutual agreement ensures their identical properties, and the simulated data have been incorporated for comparison, indicating a very close agreement with the measurements.

The radiation characteristics of the prototype have been measured using the limited facilities available in the chamber and have, therefore, been restricted to two representative frequencies. Figure 9 compares the E-plane radiation characteristics obtained at 5 and 10 GHz with the simulated predictions, and a close mutual agreement is revealed. Over the band, the performance has been verified by examining the transmission coefficient for a setup shown in the inset of Figure 10. Both the measured and simulated S_{21} have been compared in Figure 10, and the numerical value is a function of their separation r. The measurement closely follows the simulated curve and ensures their consistent radiation over the wide bandwidth.

VERIFIED IN THE TIME DOMAIN

Time-domain studies have been executed in terms of the transient response in transmit and receive modes with a monocycle pulse as the input. It has been chosen as 160 ps, following the recent studies described in [11]. The resulting radiated pulse has been received using a field probe [13] and identified as the inverted second temporal derivative of the input, which ensures UWB characteristics [11]. When this antenna is used in the receiving mode with a plane wave monocycle incidence, its received signal represents the first temporal derivative of the monocycle, which also ensures the desired characteristics.

Figure 11(a) shows the calculated group delay. The maximum of 1.6 ns, occurring at 20 and 25 GHz, correlates two specific higher order modes. The impulse response $h(t)$ of the DRA can be determined numerically from S_{21} (Figure 10) using a Fourier transform. Then, by convoluting it with the incident pulse $x(t)$, one can obtain the radiated pulse $y(t) = x(t) * h(t)$ as shown by the dotted curve in Figure 11(b). This numerically obtained $y(t)$ closely corroborates the solid curve, obtained by electromagnetic simulation [13]. Their relative dis- placement in the time scale is due to the fact that the dotted curve is based on S_{21} data, which account for the transmission time, but such a consideration is absent in determining the solid curve. The difference between their amplitudes is just a numerical factor. Therefore, their close agreement in terms of time- domain response is highly significant, ensuring the UWB operation of the proposed antenna.

CONCLUSIONS

The vertical alignment of the DRR blocks is a bit tricky, but it is not a difficult task. However, maintaining accuracy during the preparation of the dices and composites for the DRR units appears to be a challenging job. Yet, this examination has successfully demonstrated an excellent accuracy through a series of experiments. This should give confidence to DRA researchers to use such composite materials and configurations for advanced designs and applications.

REFERENCES

[1] M. Lapierre, Y. M. M. Antar, A. Ittipiboon, and A. Petosa, "Ultrawideband monopole/dielectric resonator antenna," *IEEE Microw. Compon. Lett.*, vol. 15, no. 1, pp. 7–9, Jan. 2005.

[2] D. Guha, Y. M. M. Antar, A. Ittipiboon, A. Petosa, and D. Lee, "Improved design guidelines for the ultra wideband monopole-dielectric reso- nator antenna," *IEEE Antennas Wireless Propag. Lett.*, vol. 5, no. 1, pp. 373–377, Dec. 2006.

[3] S. Thirakoune, A. Petosa, and A. Ittipiboon, "Yagi-like DRA-loaded monopole," in *Proc. Int. Conf. Electromagnetics Advanced Applications*, 2007, pp. 1–4.

[4] S. Ghosh and A. Chakrabarty, "Ultrawideband performance of dielectric loaded T-shaped mono- pole transmit and receive antenna/EMI sensor," *IEEE Antennas Wireless Propag. Lett.*, vol. 7, pp. 358–361, Mar. 2008.

[5] M. N. Jazi and T. A. Denidni, "A new hybrid skirt monopole dielectric resonator antenna," in *Proc. IEEE Antennas and Propagation Society Int. Symp*., 2008, pp. 1–4.

[6] D. Guha, B. Gupta, and Y. M. M. Antar, "New pawn-shaped dielectric ring resonator loaded hybrid monopole antenna for improved ultrawide bandwidth," *IEEE Antennas Wireless Propag. Lett.*, vol. 8, pp. 1178–1181, Oct. 2009.

[7] D. Guha, B. Gupta, and Y. M. M. Antar, "Hybrid monopole-DRAs using hemispherical/ conical-shaped dielectric ring resonators: Improved ultrawideband designs," *IEEE Trans. Antennas Propag.*, vol. 60, no. 1, pp. 393–398, Jan. 2012.

[8] C. Ozzaim, S. Ustuner, and N. Tarim, "Stacked conical ring dielectric resonator antenna excited by a monopole for improved ultrawide bandwidth," *IEEE Trans. Antennas Propag.*, vol. 61, no. 3, pp. 1435–1438, Nov. 2012.

[9] C. Ozzaim, "Monopole antenna loaded by stacked annular ring dielectric resonators for ultra- wide bandwidth," *Microw. Opt. Technol. Lett.*, vol. 56, no. 10, Oct. 2014.

[10] M. T. Sebastian, *Dielectric materials for wireless communications.* Oxford, U.K.: Elsevier, 2008. [11] D. Ganguly, D. Guha, S. Das, and A. Rojatkar, "Systematic approach to estimating monocycle pulse for time domain studies of UWB anten- nas using numerical computations and simulation tools," *IEEE Antennas Propag. Mag.*, vol. 56, no. 4, pp. 73–87, Aug. 2014.

[12] ANSYS. (2010). Ansoft High Frequency Structure Simulator, version 13. [Online]. Avail- able: http://www.ansys.com/About-ANSYS/News- Center/10-26-10-ANSYS-13-0-R-Built-for-Fidelity-Speed-and-Power

[13] Computer Simulation Technology. (2012). CST Microwave Studio Suite. [Online]. Available: https://www.cst.com/products/CSTMWS/

TABLE 1, THE CHRONOLOGY OF HYBRID UWB MONOPOLE-TYPE DIELECTIC RESONATOR ANTENNAS (DRAs).

Improvised Structures	DRR Unit	Bandwidth (%)	Gain (dBi)
Annular DRR (f_r = 10) loaded monopole [1]–[2]	1	100	4
Inverted conical DRR (f_r = 10) loaded monopole + skirt-shaped ground plane [5]	1	111	*
Annular DRR loaded t-shaped monopole [4]	1	112	2
Pawn-shaped DRR loaded monopole [6]	2	122	4-6
Conical and hemispherical DRA loaded monopole [7]	1	126	4-5
Stacked conical DRR [8]	2	138	8
Stacked annular DRR [9]	2	140	1-4

(* Not available)

FIGURE 1. The present geometry conceived as a combination of other geometries.

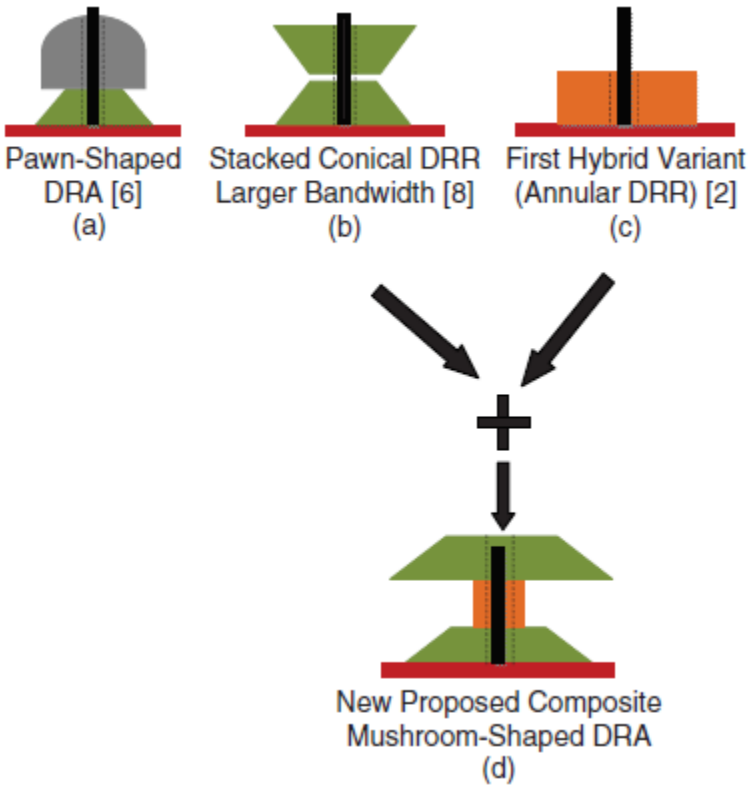

FIGURE 2. The proposed mushroom-shaped monopole-DRA for UWB operation; a cross-sectional view.

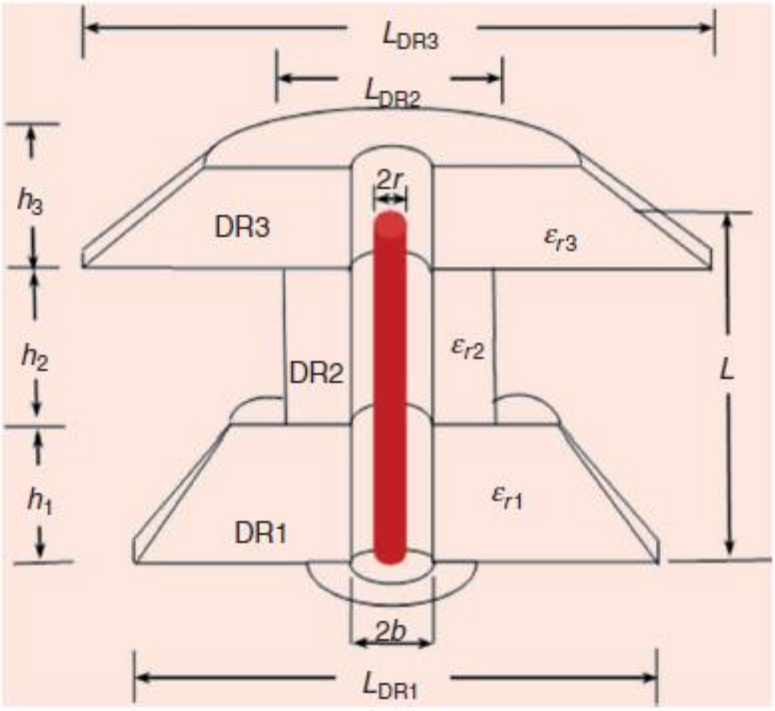

FIGURE 3. The simulated S_{11} characteristics for different resonating units (arrows depict correspondence in between the resonant modes) with *h*1 =4, *h*2 =5, *h*3 =4, *L*DR1 =18, *L*DR2 =6, *L*DR3 =22, *b* =1.5, *fr*1 =7, *fr*2 =5, *fr*2 =4, and *l* =11. (All dimensions are in millimeters.)

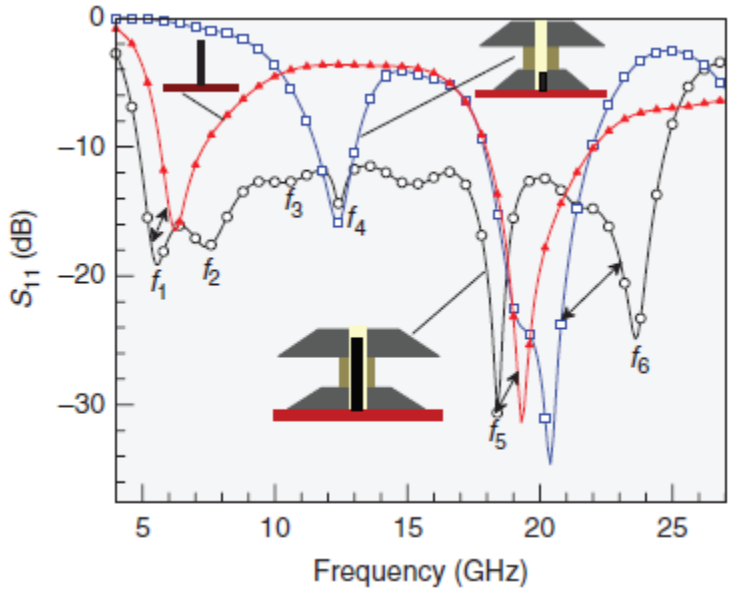

FIGURE 4. The simulated S_{11} characteristics of the monopole loaded by different blocks of the DRR.

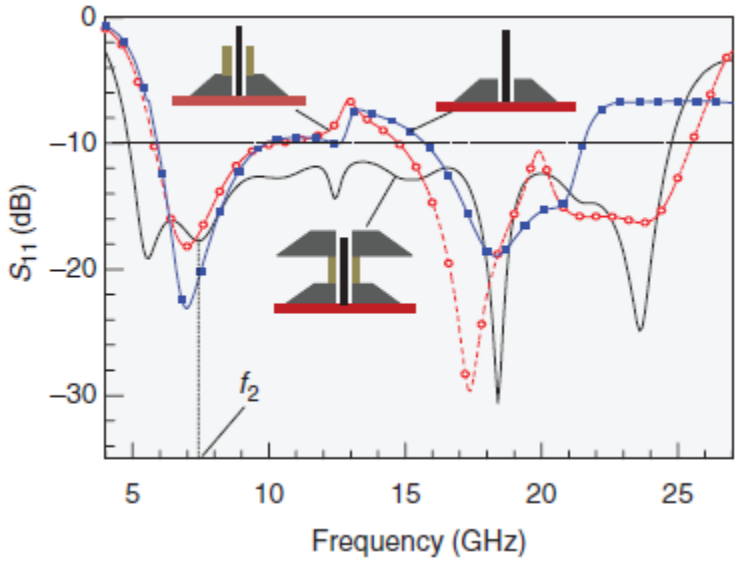

FIGURE 5. The surface current on the monopole as a function of DRR loading: (a) f_2 at 7.3 GHz, l_{eq} .0.93l; (b) f_3 at 10.3 GHz, l_{eq} .0.67l. The maximum current density represented by red (in color) and light gray (in black and white) and minimum by blue (in color) and deep gray (in black and white). The parameters used are the same as those used in Figure 3.

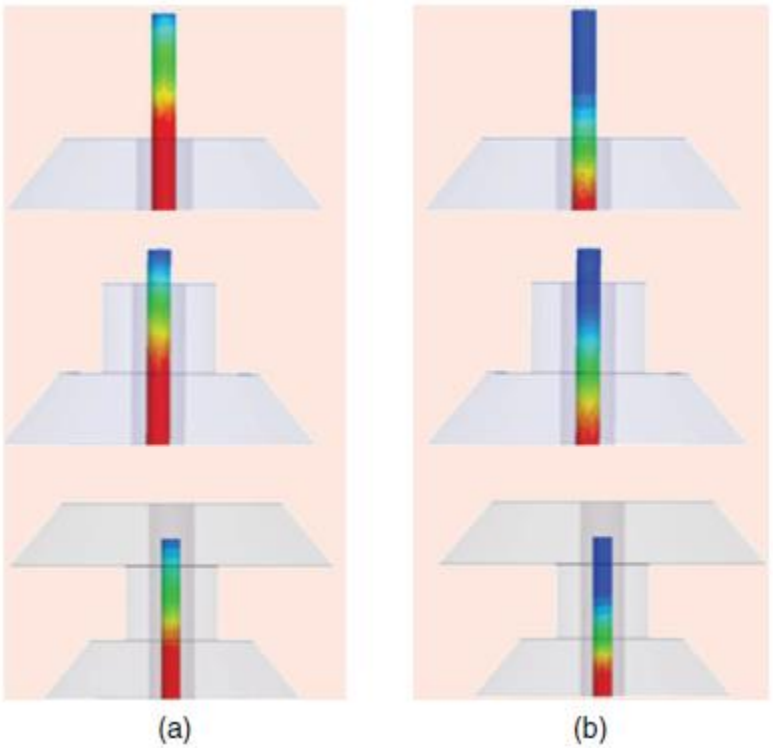

FIGURE 6. The E-plane radiation pattern showing a peak gain at different frequencies. The parameters used are the same as those used in Figure 3.

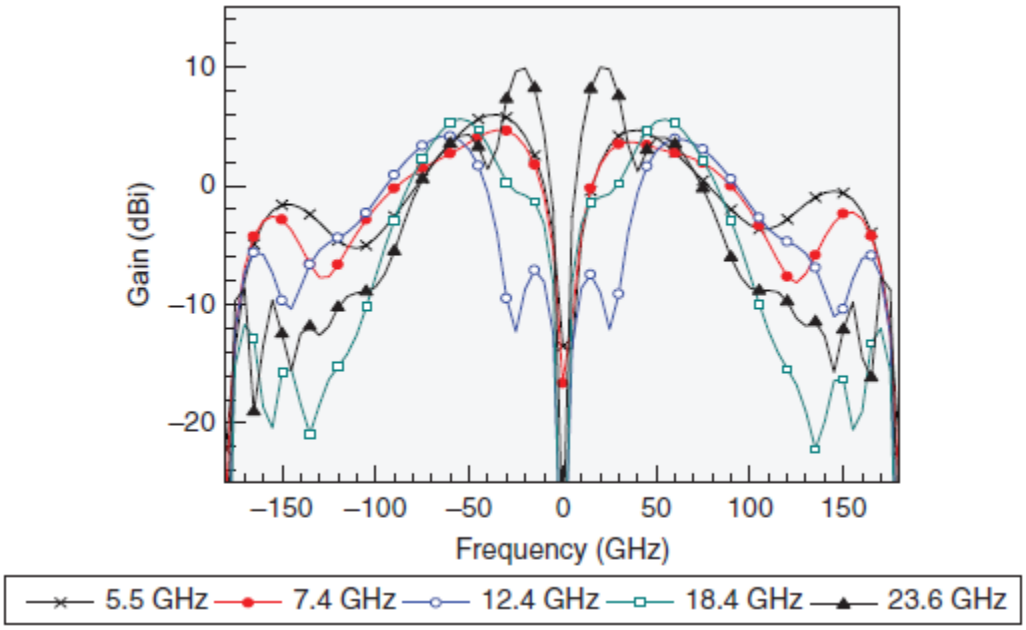

FIGURE 7. The fabricated mushroom-shaped DRA with $h1$ =4.2, $h2$ =5.1, $h3$ =4.2, LDR1 =17.6, LDR2 =6, LDR3 =22.2, b =1.57, $fr1$ =6.5, $fr2$ =4.5, $fr2$ =4, and l =11. (All dimensions are in millimeters.)

FIGURE 8. The simulated and measured return loss characteristics for mushroom prototypes shown in Figure 8. The parameters used are the same as those used in Figure 3 (simulated) and Figure 7 (measured).

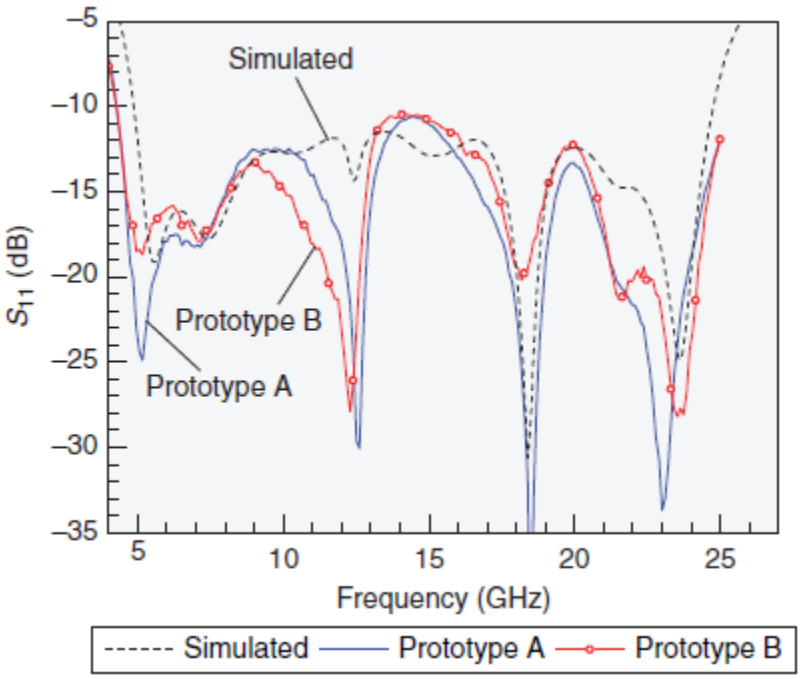

FIGURE 9. The measured E-plane radiation plot obtained at (a) 5 GHz and (b) 10 GHz. The parameters used are the same as those used in Figure 7.

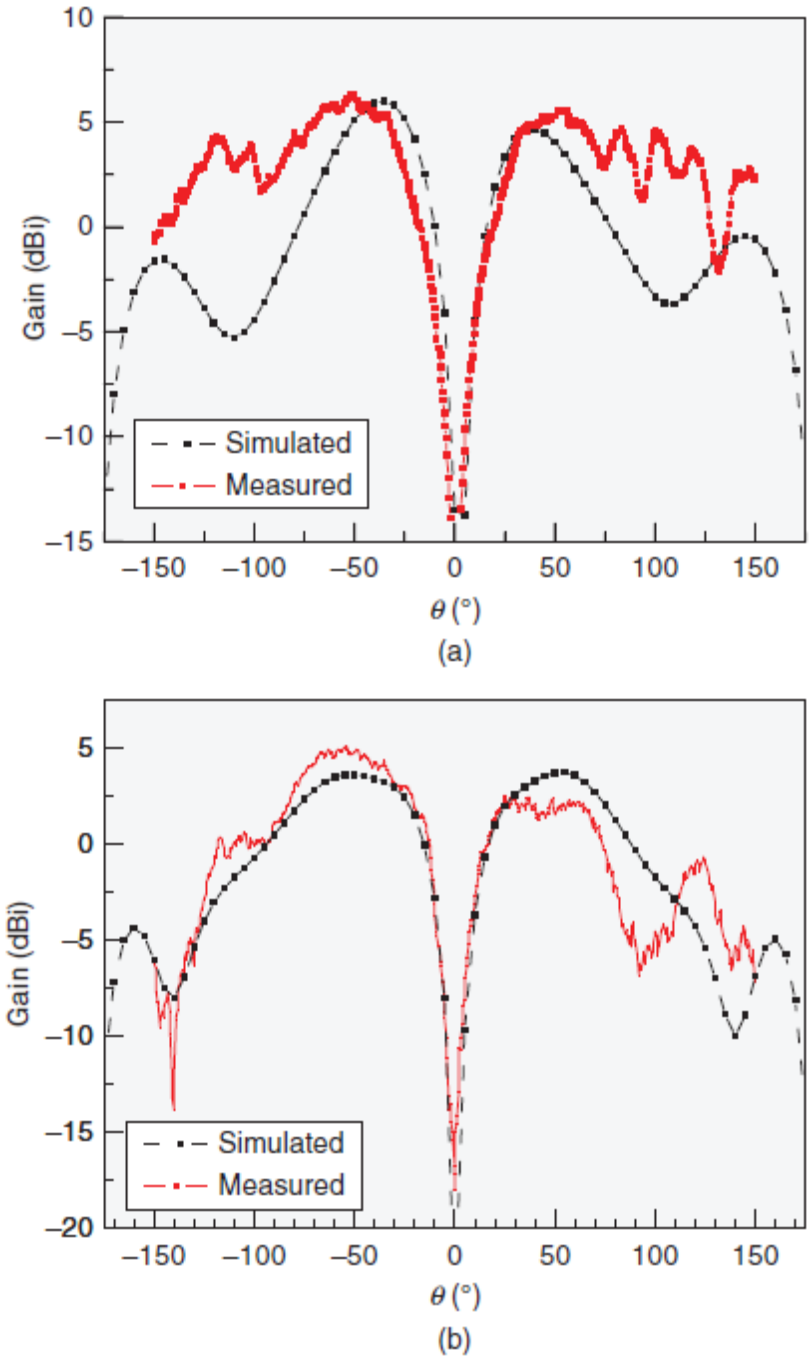

FIGURE 10. The plot of measured and simulated transmission characteristics (S_{21}) in the operating bandwidth. Two antenna units under test for S_{21} measurement maintaining their separation *r* 2^2^*h*1 +*h*2 +*h*3h2/*m*h in the inset. The parameters used are the same as those used in Figures 3 and 7.

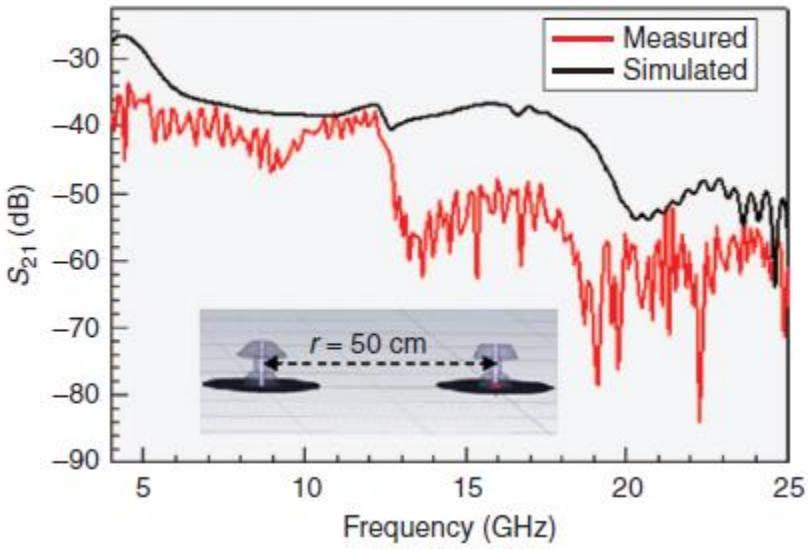

FIGURE 11. The simulated and computed characteristics: (a) the group delay over the band and (b) the response in receiving mode for a monocycle impulse as the input (computed field accounts for the inherent time delay in S_{21}). The parameters used are the same as those used in Figure 3.